Article

# Catalogue of flat-band stoichiometric materials

https://doi.org/10.1038/s41586-022-04519-1

Received: 8 June 2021

Accepted: 4 February 2022

Published online: 30 March 2022

Check for updates

Nicolas Regnault[1,2,11]✉, Yuanfeng Xu[3,11]✉, Ming-Rui Li[4,11], Da-Shuai Ma[5,11], Milena Jovanovic[6], Ali Yazdani[1], Stuart S. P. Parkin[3], Claudia Felser[7], Leslie M. Schoop[6], N. Phuan Ong[1], Robert J. Cava[6], Luis Elcoro[8,11], Zhi-Da Song[1,11] & B. Andrei Bernevig[1,9,10,11]✉

Topological electronic flattened bands near or at the Fermi level are a promising route towards unconventional superconductivity and correlated insulating states. However, the related experiments are mostly limited to engineered materials, such as moiré systems[1–3]. Here we present a catalogue of the naturally occuring three-dimensional stoichiometric materials with flat bands around the Fermi level. We consider 55,206 materials from the Inorganic Crystal Structure Database catalogued using the Topological Quantum Chemistry website[4,5], which provides their structural parameters, space group, band structure, density of states and topological characterization. We combine several direct signatures and properties of band flatness with a high-throughput analysis of all crystal structures. In particular, we identify materials hosting line-graph or bipartite sublattices—in either two or three dimensions—that probably lead to flat bands. From this trove of information, we create the Materials Flatband Database website, a powerful search engine for future theoretical and experimental studies. We use the database to extract a curated list of 2,379 high-quality flat-band materials, from which we identify 345 promising candidates that potentially host flat bands with charge centres that are not strongly localized on the atomic sites. We showcase five representative materials and provide a theoretical explanation for the origin of their flat bands close to the Fermi energy using the *S*-matrix method introduced in a parallel work[6].

Electrons whose energy dispersion is bound within a narrow window are conjectured to show a wide range of interesting physics phenomena. Such electrons form a high density of states 'flat band', where many-body effects dominate over the kinetic energy and where Fermi-surface physics gives way to strongly interacting, non-Fermi liquid behaviour[7]. The archetypal—and until recently the only experimentally discovered—system is the fractional quantum Hall effect[8,9] where anyonic (potentially non-Abelian[10]) quasiparticle excitations can appear under a fractional filling of an electronic flat band that develops in the presence of a large magnetic field. Developments in engineered solid-state materials have now shown that flat bands can exist even in the absence of a large magnetic field. In moiré materials such as (but not limited to) twisted bilayer graphene (TBG)[1–3], flat electronic bands are obtained by creating large, many nanometre-size moiré unit cells, which folds and flattens the initial band structure of the material. This flatness has a crucial role in the physics of TBG, leading to, for example, both the correlated insulator states and the strong-coupling superconductivity that renders the TBG phase diagram akin to that of the high-temperature cuprates. However, as the unit cell is large, the electron density in moiré samples is necessarily low, which prevents the type of physics associated with high electron density[11,12]. This renders the yet elusive prediction of flat bands in non-moiré, stoichiometric crystals of immediate importance.

Here we address the question of predicting and classifying the flat bands in the stoichiometric crystals currently present in nature, keeping in mind that not all flat bands are created equal. Extremely localized orbitals—or large unit cells with well separated atoms—can easily give rise to mundane flat atomic bands (FABs), as the kinetic energy is suppressed by the vanishing overlap between atomic wavefunctions, as schematically shown in Fig. 1a. FABs are common in layered and heavy fermion systems. At the opposite side of the spectrum are the flat topological bands (FTBs) created by completely extended wavefunctions (such as is the case in TBG), as schematically shown in Fig. 1b. (See Supplementary Section B for a more detailed discussion of the FABs and FTBs.) There, the quenching of the kinetic energy arises from interference effects despite large electron orbital overlaps and hopping. FTBs can host many exotic quantum phenomena, including magnetism, the fractional quantum Hall effect at zero field[13–16], unconventional superconductivity[2,17,18], non-Fermi liquid behaviour[7] and anomalous Landau levels beyond Onsager's rule[19]. Such topological

[1]Department of Physics, Princeton University, Princeton, NJ, USA. [2]Laboratoire de Physique de l'Ecole normale supérieure, ENS, Université PSL, CNRS, Sorbonne Université, Université Paris-Diderot, Sorbonne Paris Cité, Paris, France. [3]Max Planck Institute of Microstructure Physics, Halle, Germany. [4]Department of Physics, Tsinghua University, Beijing, China. [5]Beijing Key Laboratory of Nanophotonics and Ultrafine Optoelectronic Systems, School of Physics, Beijing Institute of Technology, Beijing, China. [6]Department of Chemistry, Princeton University, Princeton, NJ, USA. [7]Max Planck Institute for Chemical Physics of Solids, Dresden, Germany. [8]Department of Condensed Matter Physics, University of the Basque Country UPV/EHU, Bilbao, Spain. [9]Donostia International Physics Center, Donostia-San Sebastian, Spain. [10]IKERBASQUE, Basque Foundation for Science, Bilbao, Spain. [11]These authors contributed equally: Nicolas Regnault, Yuanfeng Xu, Ming-Rui Li, Da-Shuai Ma, Luis Elcoro, Zhi-Da Song, B. Andrei Bernevig. ✉e-mail: regnault@princeton.edu; yfxu@mpi-halle.mpg.de; bernevig@princeton.edu

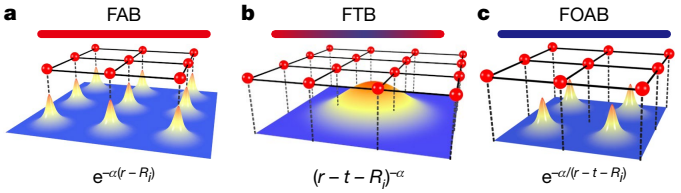


**Fig. 1 | An illustration of the three possible types of flat band. a**, FABs: the Wannier functions associated with the flat bands are exponentially localized on the atoms' sites. **b**, FTBs: the Bloch states are extended (with potentially a power-law decay) in at least one direction of the lattice. **c**, FOABs: as opposed to FABs, the corresponding Wannier functions are exponentially localized but on an empty site. The atom sites of the two-dimensional lattices are shown with red spheres. Below the lattices are the Bloch wave functions at position $r$ of the flat bands associated with their decay law, where $R_i$ is the position of atom $i$, $t$ is a fractional lattice vector and $\alpha$ is a positive coefficient.

bands can enhance the superfluid weight in TBG[20,21] and could lead to high-temperature superconductivity. An ideal FTB near the Fermi level in crystalline materials has not yet been found; the only experimentally found FTBs are in engineered TBG. A third type, the flat obstructed atomic band (FOAB), lies at the interface between the polar opposites FAB and FTB: although the electron's symmetric Wannier function can be localized in real space, the Wannier center is pinned and centred at an empty site[22,23] and hence delocalized from the atomic sites, as illustrated in Fig. 1c.

We present and implement algorithms for the detection and classification of flat bands near the Fermi level. Using the materials in our Topological Quantum Chemistry Database website (TQCDB; https://www.topologicalquantumchemistry.com), which contains most of the Inorganic Crystal Structure Database (ICSD) stoichiometric structures and was obtained in previous studies[4,5,22], we build the complementary Materials Flatband Database website (MFBDB; https://www.topologicalquantumchemistry.fr/flatbands/), where different algorithms and search options for flat bands are provided to the user. First, we perform a brute-force search based on complementary 'flatness' criteria such as bandwidth and density of states (DOS), to predict all the (thousands) flat-band materials in the ICSD database. We classify these bands based on their topologies. Second, using a theory that we have developed in ref. [6] encompassing generic orbital systems with or without spin–orbit coupling (SOC), we perform a targeted search of flat-band materials based on the lattice geometry (such as Kagome, pyrochlore, Lieb, bipartite or split sublattices) of the compounds, taken from the X-ray diffraction data on TQCDB or ICSD. We show that geometry-based theoretical models based on the $S$-matrix method[6] fit our ab initio calculations of the flat bands remarkably well. Third, we perform a manual check of thousands of materials for the best flat bands and select 2,379 materials with high-quality flat bands near the Fermi level. We showcase our methods, theoretical understanding and predictive power for five representative flat-band materials, and in the Supplementary Information we present thousands of others. Our classification and predictions take into account the different flat-band natures, including their topological character, and our database is coupled to the Materials Project (https://materialsproject.org/) and NIMS Materials Database (https://mits.nims.go.jp/en/), providing information about the magnetic and superconducting properties (including high-temperature superconductivity) of the candidate materials.

## Database of flat-band materials

Here we have used the TQCDB[4,5] as our materials database. We summarize its main features in Methods and provide a detailed overview in Supplementary Section C1. As we are interested in flat bands near the Fermi energy, we discard materials containing rare-earth elements (with the exception of the lanthanum atom) and actinides as these elements usually lead to spurious flat bands owing to $f$ electrons in the ab initio calculations. In total, 55,206 ICSD entries were considered for our high-throughput search for flat bands. The automated search is based on two main, complementary, approaches: the detection of flat bands in the band structure and the DOS, and the identification of special sublattices that lead to band flattening. We now detail each of them.

### High-throughput search for flat bands

To determine band flatness, we rely on calculations where the SOC is neglected. Although SOC has an important role in the topological features near the Fermi level, it does not drastically affect the band structure nor the DOS around the Fermi energy $E_F = \pm 2$ eV region where we focus our search. For each ICSD entry, our database provides the ab initio paramagnetic-phase electronic band structure along paths made of straight lines in the Brillouin zone connecting high-symmetry points ('high-symmetry lines'). Each high-symmetry line is well defined in every space group (SG) and it has been discretized, irrespective of its length, into 20 equally distant $k$-points (that is, points in the Brillouin zone). As we are interested in low-energy physics, we focus our investigations on the flatness of the two highest/lowest occupied/empty bands around $E_F$, which is reached when the occupation number of bands equals half the number of valence electrons. Although paramagnetic calculations would fail to capture (anti-)ferromagnetic ground states, we discuss four representative ferromagnetic compounds in Supplementary Section G. Our ferromagnetic calculations both match the experimental results and, while preserving the flat bands obtained in the paramagnetic calculations, remain near the Fermi level.

As motivated in Supplementary Section I, we investigate bands that are flat in parts of the (but not necessarily over the entire) Brillouin zone. Thus for each ICSD entry, we search for flat-band segments: a series of $L$ consecutive $k$-points along the high-symmetry lines of the band structure (we use $L = 10$, $L = 20$, $L = 30$, $L = 40$ or $L = 50$), where the energy band width is smaller than a tunable threshold $\omega$ (ranging from 25 meV to 150 meV). The number of such flat segments for every band analysed provides a convenient signature of band flatness. In Supplementary Section C2a, we provide a full discussion of the definition, the algorithm and the statistics of flat-band segments around $E_F$.

The presence of a flat-band segment alone is not sufficient to predict the presence of interesting physics associated with it: a (quasi) one-dimensional system would equally show a flat-band segment in the directions perpendicular to its dispersive direction. However, peaks (or their absence) in the DOS offer a simple and efficient way to filter out such pathological cases. Thus for each ICSD entry, we map the position and width of all DOS peaks in an energy region of ±5 eV around $E_F$. More details about the DOS peak detection are given in Supplementary Section C2b.

### Automated identification of sublattices

Geometric frustration in (line-graph and bipartite) lattices is known to give rise to exact FTBs[24–29]. Although initially predicted for $s$ orbitals, this property was recently generalized to a slew of other possible orbital–lattice combinations[6]. This provides a crucial starting point to understand and predict flat bands in crystalline materials: if a material hosts a line-graph or bipartite lattice as a part of its lattice structure (a 'sublattice'), and if this sublattice is only weakly perturbed or deformed by the remaining atoms or orbitals, we expect to observe FTBs. To explain the origin of the flat bands found in our high-throughput search, we have automated, using the structural parameters of every ICSD entry, the detection of five types of line-graph or bipartite sublattice: the Kagome, pyrochlore, Lieb, bipartite or split sublattices as detailed in Supplementary Sections D, E.

In three dimensions, the Kagome, pyrochlore and Lieb lattices can be mathematically characterized by special occupied Wyckoff positions in certain SGs. Using the crystalline structures of materials, we

**Table 1 | Statistics of the ICSD entries in the database hosting at least one sublattice for each lattice type**

| | All ICSDs | Curated | Best |
|---|---|---|---|
| Number of ICSDs | 55,206 | 6,338 | 949 |
| Number of materials | 28,169 | 2,379 | 345 |
| Kagome | 6,120 (11.09%) | 1,699 (26.81%) | 516 (54.37%) |
| Pyrochlore | 1,666 (3.02%) | 296 (4.67%) | 77 (8.11%) |
| Lieb | 1,590 (2.88%) | 721 (11.38%) | 151 (15.91%) |
| Bipartite | 21,175 (38.36%) | 3,138 (49.51%) | 432 (45.52%) |
| Split | 8,224 (14.90%) | 1,920 (30.29%) | 354 (37.30%) |
| None | 31,154 (56.43%) | 2,582 (40.74%) | 248 (26.13%) |

In the first row, we give the number of ICSD entries for the database (first column), for the list of curated flat-band materials (second column) and for the best representative flat-band materials (third column). The second line provides the number of unique materials for the database, the list of curated flat-band materials and the best representative flat-band materials. The third, fourth, fifth, sixth and seventh rows are the statistics for the Kagome, pyrochlore, Lieb, bipartite (with different numbers of atoms on sublattices) and split lattices, respectively. An ICSD entry is considered as hosting a given type of lattice if the algorithms discussed in Supplementary Section IIB have found at least one such lattice irrespective of the cut-offs or being a rigourous or approximate sublattice. Note that an ICSD entry might host more than one type of sublattice. The eighth row provides the statistics for the ICSDs where no sublattices have been detected. For each column, the percentages are calcuated with respect to the number of ICSDs provided in the first row.

have developed an SG method to detect the line-graph and Lieb sublattices (Methods). Although the SG method provides a fast way to find the symmetric Kagome, pyrochlore and Lieb sublattices in crystalline materials, the exact sublattice might be spoiled by the presence of other atoms of the same element on (or close to) this sublattice. Moreover, the SG method discards approximate sublattices, which could also exhibit quasi-flat bands. To solve these issues, we have further developed a geometric method that solely relies on the geometric features of these three sublattice types (discussed in Supplementary Section D2) and ignores the exact SG restrictions. In Supplementary Section D3, we provide a detailed presentation of our algorithms implementing the geometric method for each type of sublattice. Equipped with these methods, we sort all the possible sublattices in a material in two categories: the rigorous sublattices, which satisfy both methods, and the approximate sublattices, which satisfy only the geometric method but capture weak distortions of rigorous sublattices.

A bipartite lattice with chiral symmetry is formed by two sublattices L and $\tilde{\mathrm{L}}$ with the kinetic hopping only between L and $\tilde{\mathrm{L}}$. As proposed in ref. [6] and briefly introduced in Methods and Supplementary Section E1, a general method, namely the *S*-matrix method, can be used to explain the origin of flat bands in crystalline materials whose lattice contains a bipartite or split sublattice. We have developed an algorithm (detailed in Supplementary Section E) to search for bipartite lattices from the structural parameters of each ICSD entry with the following necessary simplifying assumptions for a high-throughput analysis. For each crystal structure in the MFBDB, we solely rely on the geometric distance between two atoms to infer the amplitude of kinetic hopping between them. By ignoring the small hopping terms based on a tunable cut-off, we identify whether a crystalline material has a bipartite sublattice with a different number of atoms in its L and $\tilde{\mathrm{L}}$ sublattices. In the algorithm, a special case of bipartite sublattice, namely the split sublattice, which has been proposed to host FTBs[28], is also detected and tagged.

## High-throughput search results

We now summarize the main results obtained in the present high-throughput search. First, we discuss the number of geometric sublattices detected by our algorithms and the public website we have developed to search for materials with flat bands based on the criterion in Supplementary Section II. We discuss a manually curated list of 2,379 materials potentially hosting FTBs, obtained using our toolset. Then, we showcase the five best representative flat-band materials and explain the flat-band segments in their band structures using the *S*-matrix method[6].

### Statistics and website

By applying the automated analysis of the lattice structure to the 55,206 ICSD entries of the MFBDB, we have performed a high-throughput search of the rigorous and approximate Kagome, Lieb and pyrochlore sublattices, and the bipartite/split lattice with different numbers of atoms on their further sublattices. We found 6,120 ICSDs with at least one Kagome (rigorous or approximate) sublattice, including 4,192 ICSDs with a Kagome sublattice labelled as rigorous, 1,666 ICSDs with a pyrochlore sublattice (rigorous or approximate) and 1,541 ICSDs with a rigorous pyrochlore sublattice. For the Lieb lattice, there are 1,590 ICSDs hosting such a sublattice, including 1,202 ICSDs with rigorous Lieb sublattices. At least one bipartite sublattice (irrespective of the cut-offs) is found among 21,175 ICSDs and split sublattices are found in 8,224 ICSDs. A breakdown of these statistics per SG is provided in Supplemenatry Section C3. The brute-force scan of the band structures along the high-symmetry lines was performed for several threshold parameters. The number of ICSDs exhibiting flat-band segments varies strongly on these parameters; for a detailed statistical analysis, see Supplemenatry Section C2a.

The data generated through the automated algorithms discussed in Supplemenatry Section II are available through our MFBDB (see Supplemenatry Section C2 for an overview of the search engine). We used this website to perform an extensive investigation of promising candidate materials exhibiting flat bands or a large segment of flat bands close to the Fermi energy. The outcome of our search is provided as a list of curated flat-band materials in Supplemenatry Section H1. This list contains 6,338 ICSD entries that can be regrouped into 2,379 unique materials, that is, ICSDs sharing the same stoichiometric formula, SG and topological properties at the Fermi energy (as defined in Supplemenatry Section C1). The complete set of criteria applied to select these materials is provided in Supplemenatry Section H1, and it includes the distance to the Fermi energy, the flat band width and topology, and the presence of a peak in the DOS. We have excluded cases where the flat bands were clear FABs from the list of curated flat-band materials, and they are listed in Supplemenatry Section H2. The statistics of detected sublattices among the curated materials are provided in Table 1.

### Flat-band material candidates

Among the 2,379 high-quality flat-band materials, we select 345 best representative flat-band materials in Supplemenatry Section H3 for further experimental investigation. Most of the 345 materials host one (or more than one) of the Kagome, pyrochlore, Lieb, bipartite and split sublattices in their crystal structures. For each of the five types of sublattice, we select one representative material that hosts the best flat-band segments on (or close to) the Fermi level, and explain its physical origin using the *S*-matrix method[6]. All of the five representative flat-band materials are chemically realistic, experimentally paramagnetic and not Mott insulators, which is consistent with our paramagnetic calculations.

The five typical materials are $KAg(CN)_2$ (ICSD 30275, SG 163 ($P\bar{3}1c$)) with an approximate Kagome sublattice formed by silver atoms, $Pb_2Sb_2O_7$ (ICSD 27120, SG 227 ($Fd\bar{3}m$)) with a pyrochlore sublattice formed by lead atoms, $Rb_2CaH_4$ (ICSD 65196, SG 139 ($I4/mmm$)) with a Lieb sublattice formed by calcium and hydrogen atoms, $Ca_2NCl$ (ICSD 62555, SG 166 ($R\bar{3}m$)) with a bipartite sublattice formed by calcium and nitrogen atoms, and $WO_3$ (ICSD 108651, SG 221 ($Pm\bar{3}m$)) with a split sublattice formed by tungesten and oxygen atoms. Their crystal structures are shown in Fig. 2a–e and the orbital characters of the flat bands

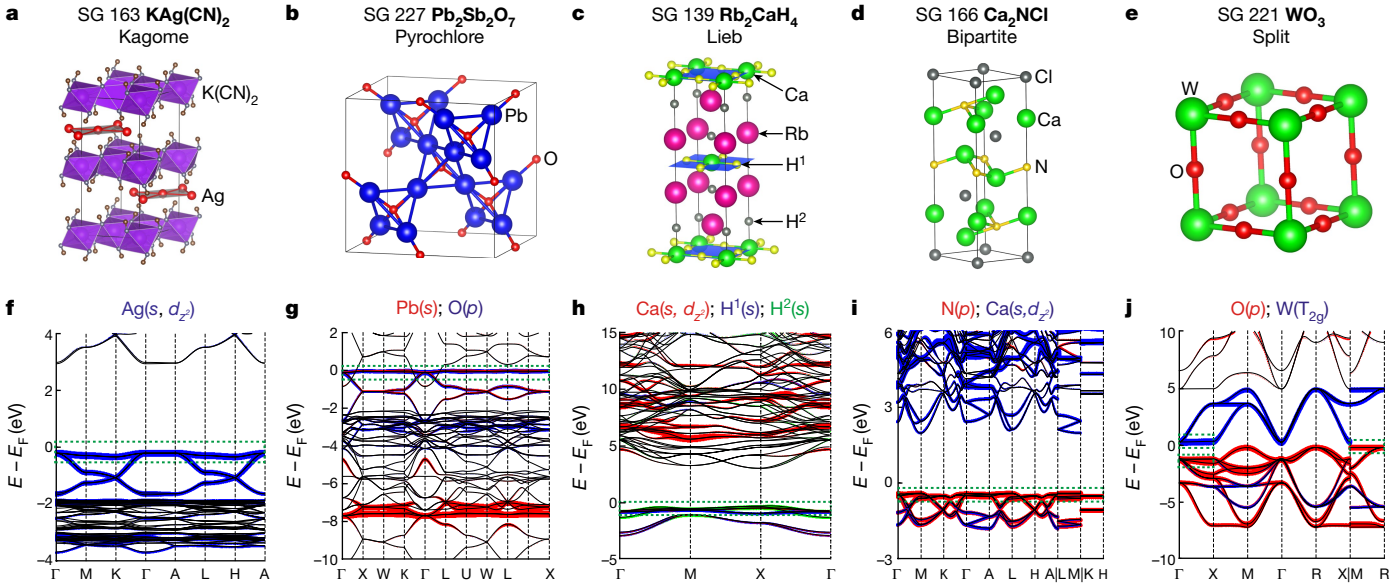


**Fig. 2 | Crystal and band structures of the representative flat-band materials. a**–**e**, The crystal structures of $KAg(CN)_2$ (**a**), which hosts an approximate Kagome sublattice formed by the Ag atoms (in red), $Pb_2Sb_2O_7$ (**b**) with Pb atoms at the Wyckoff position 16*d* forming a pyrochlore sublattice, $Rb_2CaH_4$ (**c**) with the H atoms at 4*c* (that is, the $H^1$ atoms in yellow) and the Ca atoms at the 2*a* position forming a Lieb sublattice, $Ca_2NCl$ (**d**), which is stacked by alternating the $Ca_2N$ and Cl layers, where the $Ca_2N$ layer is identified as a bipartite sublattice in our algorithm, and $WO_3$ (**e**) with the W and O atoms forming a split lattice. **f**–**j**, For each material, its band structure and the orbital characterization of the flat bands is plotted and analysed below its crystal structure. On the basis of the band structure analysis, the flat bands close to the Fermi level are explained by the *S*-matrix method in Supplemtary Section F. In the crystal structure plots, the SG, chemical formula and the type of sublattice host in the material are provided at the top of each panel. In the band-structure plots, the flat-band segments close to the Fermi level are indicated by the dashed green lines. The orbital characters of the coloured bands are provided at the top of each panel.

in the five materials are shown in the orbital-projected band structures in Fig. 2f–j. As detailed in Supplemenatry Section F, on the basis of the crystal structure and orbital-projected bands of these materials, we have constructed effective tight-binding Hamiltonians using the *S*-matrix method[6] and found that they can successfully explain the origins of flat bands. The flat bands of other materials of similar crystal structures can be found in the MFBDB. In Methods, we use $Ca_2NCl$ to showcase the application of the *S*-matrix method in explaining the origin of flat bands.

## Discussion

We have performed a high-throughput search for flat electronic bands near the Fermi level and for the detection of line-graph and bipartite sublattices from the crystal structures of stoichiometric crystalline materials. We have further classified the flat bands by their topology, DOS, length of band flatness and the types of lattice formed by the atoms whose orbitals contribute to the flat band. By successfully applying our algorithms to 55,206 ICSD entries, we have found that 24,052 (43.57%) out of all the ICSD entries host at least one of the Kagome, pyrochlore, Lieb, bipartite or split sublattices in their crystal structures. This proportion is raised to 59.26% for our manually curated list of 6,338 ICSDs (2,379 unique materials) and 73.87% for the best representative flat-band materials. The appearance of flat bands in materials can be, in large but non-exhaustive part, theoretically understood using the *S*-matrix method[6], as we have exemplified in five prototypical compounds. All the results obtained in this study and detailed in the Supplementary Information can be accessed on the MFBDB. Our results pave the way for future theoretical and experimental studies on flat-band materials combining topology and interactions and leading to exotic quantum phenomena, such as magnetism, non-Fermi liquid behaviour and superconductivity. Such flat-band investigations are, at present, confined to engineered twisted moire lattices in two dimensions. Although the present work studies flat bands in paramagnetic band structures of three-dimensional materials, our methods can be adapted to detect flat bands in magnetic band structures, two-dimensional monolayer materials, phonons and photonic crystals. Furthermore, the further classification of FOABs will enlarge the set of flat bands whose centre of charge is away from the atomic positions.

## Online content

Any methods, additional references, Nature Research reporting summaries, source data, extended data, supplementary information, acknowledgements, peer review information; details of author contributions and competing interests; and statements of data and code availability are available at https://doi.org/10.1038/s41586-022-04519-1.


1. Bistritzer, R. & MacDonald, A. H. Moiré bands in twisted double-layer graphene. *Proc. Natl Acad. Sci. USA* **108**, 12233–12237 (2011).
2. Cao, Y. et al. Unconventional superconductivity in magic-angle graphene superlattices. *Nature* **556**, 43–50 (2018).
3. Cao, Y. et al. Correlated insulator behaviour at half-filling in magic-angle graphene superlattices. *Nature* **556**, 80–84 (2018).
4. Vergniory, M. G. et al. A complete catalogue of high-quality topological materials. *Nature* **566**, 480–485 (2019).
5. Vergniory, M. G. et al. All topological bands of all stoichiometric materials. Preprint at https://arxiv.org/abs/2105.09954 (2021).
6. Călugăru, D. et al. General construction and topological classification of crystalline flat bands. *Nat. Phys.* **18**, 185–189 (2022).
7. Kumar, P., Peotta, S., Takasu, Y., Takahashi, Y. & Törmä, P. Flat-band-induced non-Fermi-liquid behavior of multicomponent fermions. *Phys. Rev. A* **103**, L031301 (2021).
8. Tsui, D. C., Stormer, H. L. & Gossard, A. C. Two-dimensional magnetotransport in the extreme quantum limit. *Phys. Rev. Lett.* **48**, 1559–1562 (1982).
9. Laughlin, R. B. Anomalous quantum Hall effect: an incompressible quantum fluid with fractionally charged excitations. *Phys. Rev. Lett.* **50**, 1395–1398 (1983).
10. Moore, G. & Read, N. Nonabelions in the fractional quantum Hall effect. *Nucl. Phys. B* **360**, 362–396 (1991).
11. Drozdov, A., Eremets, M., Troyan, I., Ksenofontov, V. & Shylin, S. I. Conventional superconductivity at 203 kelvin at high pressures in the sulfur hydride system. *Nature* **525**, 73–76 (2015).

12. Drozdov, A. et al. Superconductivity at 250 K in lanthanum hydride under high pressures. *Nature* **569**, 528–531 (2019).
13. Tang, E., Mei, J.-W. & Wen, X.-G. High-temperature fractional quantum Hall states. *Phys. Rev. Lett.* **106**, 236802 (2011).
14. Neupert, T., Santos, L., Chamon, C. & Mudry, C. Fractional quantum Hall states at zero magnetic field. *Phys. Rev. Lett.* **106**, 236804 (2011).
15. Sheng, D., Gu, Z.-C., Sun, K. & Sheng, L. Fractional quantum Hall effect in the absence of Landau levels. *Nat. Commun.* **2**, 389 (2011).
16. Regnault, N. & Bernevig, B. A. Fractional Chern insulator. *Phys. Rev. X* **1**, 021014 (2011).
17. Balents, L., Dean, C. R., Efetov, D. K. & Young, A. F. Superconductivity and strong correlations in moiré flat bands. *Nat. Phys.* **16**, 725–733 (2020).
18. Peri, V., Song, Z.-D., Bernevig, B. A. & Huber, S. D. Fragile topology and flat-band superconductivity in the strong-coupling regime. *Phys. Rev. Lett.* **126**, 027002 (2021).
19. Rhim, J.-W., Kim, K. & Yang, B.-J. Quantum distance and anomalous Landau levels of flat bands. *Nature* **584**, 59–63 (2020).
20. Xie, F., Song, Z., Lian, B. & Bernevig, B. A. Topology-bounded superfluid weight in twisted bilayer graphene. *Phys. Rev. Lett.* **124**, 167002 (2020).
21. Peotta, S. & Törmä, P. Superfluidity in topologically nontrivial flat bands. *Nat. Commun.* **6**, 8944 (2015).
22. Bradlyn, B. et al. Topological quantum chemistry. *Nature* **547**, 298–305 (2017).
23. Y. Xu et al. Filling-enforced obstructed atomic insulators. Preprint at https://arxiv.org/abs/2106.10276 (2021).
24. Mielke, A. Exact ground states for the Hubbard model on the kagome lattice. *J. Phys. A* **25**, 4335–4345 (1992).
25. Tasaki, H. From Nagaoka's ferromagnetism to flat-band ferromagnetism and beyond: an introduction to ferromagnetism in the Hubbard model. *Prog. Theor. Phys.* **99**, 489–548 (1998).
26. Bergman, D. L., Wu, C. & Balents, L. Band touching from real-space topology in frustrated hopping models. *Phys. Rev. B* **78**, 125104 (2008).
27. Liu, Z., Liu, F. & Wu, Y.-S. Exotic electronic states in the world of flat bands: from theory to material. *Chin. Phys. B* **23**, 077308 (2014).
28. Ma, D.-S. et al. Spin–orbit-induced topological flat bands in line and split graphs of bipartite lattices. *Phys. Rev. Lett.* **125**, 266403 (2020).
29. Chiu, C. S., Ma, D.-S., Song, Z.-D., Bernevig, B. A. & Houck, A. A. Fragile topology in line-graph lattices with two, three, or four gapped flat bands. *Phys. Rev. Res.* **2**, 043414 (2020).

# Methods

### Topological Quantum Chemistry website

The TQCDB was used as the input for the structural parameters of the stoichiometric materials reported in the ICSD[30]. For each entry, ab initio calculations were performed using density functional theory[31,32] and its implementation in the Vienna Ab-initio Simulation Package[33,34], with and without accounting for the SOC. The database provides the structural parameters, the band dispersion along high-symmetry lines, the DOS and the topological characterization for each set of bands in the material's band structure for each of the 55,206 ICSD entries.

### SG method of detecting line-graph and Lieb sublattices

To detect a Kagome, pyrochlore or Lieb sublattice in crystalline materials, we first identified the minimal SGs that support these three lattices and the corresponding Wyckoff positions (see details in Supplementary Section D1). Then, through group–subgroup relations and the split relations between the sets of Wyckoff positions on the Bilbao Crystallographic Server (https://www.cryst.ehu.es/)[35,36], we obtained all the SGs that host these lattices. The results are tabulated in Supplementary Tables IV, V in Supplementary Section D. We dub the detection of sublattices using this tabulated information as the SG method.

### A brief introduction of the *S*-matrix method

Denoting $|L|$ and $|\tilde{L}|$ as the number of atoms or orbitals in the L and $\tilde{\mathrm{L}}$ further sublattices of the bipartite or split sublattice of a material (assuming $|L| \geq |\tilde{L}|$), the Bloch Hamiltonian associated with a bipartite sublattice of a material reads

$$H(\mathbf{k}) = \begin{pmatrix} 0 & S^{\dagger}(\mathbf{k}) \\ S(\mathbf{k}) & 0 \end{pmatrix}. \quad (1)$$

Here $S(\mathbf{k})$ is a matrix with dimension $|L| \times |\tilde{L}|$ and $\mathbf{k}$ is the momentum in the Brillouin zone. A bipartite lattice with $|L| \neq |\tilde{L}|$ hosts flat bands in its band structure. For example, the Hamiltonian of equation (1) has at least $|L| + |\tilde{L}| - 2 \times \mathrm{rank}(S(\mathbf{k}))$zero-energy states, that is, the band structure has at least $|L| + |\tilde{L}| - 2 \times \mathrm{rank}(S(\mathbf{k}))$ exact flat bands. It is also likely that these bands exhibit non-trivial topology[6]. Although the other $2 \times \mathrm{rank}(S(\mathbf{k}))$ bands are dispersive, they are related by chiral symmetry. Although in real crystalline materials the chiral symmetry is generally broken by the intra-sublattice hopping, we find in ref. [6] that this *S*-matrix method goes beyond the chiral symmetry. For a generalized bipartite lattice including the intra-sublattice coupling, namely an upper (lower) diagonal block $A(k)$ ($B(k)$) in $H(k)$ for the sublattice $L(\tilde{L})$, if $A(k)$ has a momentum-independent eigenvalue $E_0$ with degeneracy $n_0$ and $|\tilde{L}| < n_0 \leq |L|$, then $H(k)$ also has at least $n_0 - |\tilde{L}|$ perfectly flat bands at energy $E = E_0$ irrespective of $B(k)$. Moreover, the eigenstates of these $n_0 - |\tilde{L}|$ flat bands are identical to those of the system with chiral symmetry[6].

### Application of the *S*-matrix method for $Ca_2NCl$

As shown in Fig. 2d, the three-dimensional crystal structure of $Ca_2NCl$ is stacked, composed of alternating $Ca_2N$ and Cl layers. In each $Ca_2N$ layer, the Ca and N atoms occupy honeycomb (with buckling) and triangular sublattices, respectively. The Cl layer also forms a triangular lattice. As shown in Fig. 2i, the flat band and the lower dispersive bands next to it are mainly contributed by the *p* orbitals of the N atoms. By constructing the maximal localized Wannier functions[37], we extract an effective tight-binding model for these *p* bands and find that its hoppings—which are computed from ab intio methods without any additional theoretical input—obey a set of fine-tuned conditions, which in turn give rise to flatness of the top *p* band. As an example, the amplitude of the σ bond is almost exactly −3 times that of the π bond. (See Supplementary Section F4 for more details.) Similar flat bands exist in many other materials of the same structure (for example, $Ca_2NBr$ and $Sr_2NCl$), and are described by similar fine-tuned ab tight-binding initio models, pointing to a deeper reason for the fine-tuning conditions.

This deep reason is the *S*-matrix theory. We notice that the nearest neighbours of the N atoms are the Ca atoms and hence that Ca and N atoms form a bipartite sublattice if only the nearest-neighbour hoppings are considered in a theoretical model of the bands. As analysed in Fig. 2i, the conduction bands around $E = 3$ eV are mainly contributed by the *s* and *d* orbitals on the Ca atoms, and the three valence bands in the energy window of roughly −3 eV to 0 eV are mainly contributed by the *p* orbitals on the N atoms and partially contributed by the hybridized orbitals consisting of *s* and $d_{z^2}$ orbitals on Ca. As the *s* and $d_{z^2}$ orbitals form the same representation ($A_1$) of the point group symmetry $C_{3v}$ isomorphic to the site-symmetry group of Ca sites, they hybridize with each other to form two hybridized orbitals. It is a reasonable simplification to take into account only the hybridized orbital with the lowest energy, which we refer to as the *s* orbital in the following. A tight-binding model including both the N and Ca atoms is naturally an *S*-matrix theory of a bipartite lattice, where the L sublattice of the bipartite (sub)-lattice consists of *p* orbitals at the triangular lattice formed by N, and the $\tilde{\mathrm{L}}$ sublattice consists of (hybridized) *s* orbitals at the honeycomb lattice (with buckling) formed by Ca. The on-site energy of *s* orbitals ($\Delta_s$) is about 3 eV. Following the argument below equation (1), there must be $|L| + |\tilde{L}| - 2 \times \mathrm{rank}(S(\mathbf{k})) = 3 + 2 - 4 = 1$ flat bands at $E = 0$. (See Supplementary Section F4 for the explicit form of $S(\mathbf{k})$.) As detailed in Supplementary Section F4, the *S*-matrix band structure matches the first-principles band structure well. Furthermore, the *S*-matrix theory also explains the fine-tuning conditions in the extracted tight-binding Hamiltonian from the maximum localized Wannier functions: the perturbative effective Hamiltonian for the *p* bands, $-S(\mathbf{k})S^{\dagger}(\mathbf{k})/\Delta_s$, perfectly reproduces the fine-tuning conditions of the ab initio model. Therefore, the *S*-matrix theory is a faithful explanation for the flat band in $Ca_2NCl$.

## Data availability

All data are available in the Supplementary Information and through our public website, the Materials Flatband Database (https://www.topologicalquantumchemistry.fr/flatbands).

## Code availability

The code developed to find the five types of sublattice mentioned herein is available from the authors upon reasonable request.


30. *Inorganic Crystal Structure Database (ICSD)* (Fachinformationszentrum Karlsruhe, 2015); https://icsd.products.fiz-karlsruhe.de/.
31. Hohenberg, P. & Kohn, W. Inhomogeneous electron gas. *Phys. Rev.* **136**, B864–B871 (1964).
32. Kohn, W. & Sham, L. J. Self-consistent equations including exchange and correlation effects. *Phys. Rev.* **140**, A1133–A1138 (1965).
33. Kresse, G. & Hafner, J. Ab initio molecular dynamics for open-shell transition metals. *Phys. Rev. B* **48**, 13115–13118 (1993).
34. Kresse, G. & Furthmüller, J. Efficiency of ab-initio total energy calculations for metals and semiconductors using a plane-wave basis set. *Comput. Mater. Sci.* **6**, 15–50 (1996).
35. Ivantchev, S., Kroumova, E., Madariaga, G., Pérez-Mato, J. M. & Aroyo, M. I. SUBGROUPGRAPH: a computer program for analysis of group–subgroup relations between space groups. *J. Appl. Crystallogr.* **33**, 1190–1191 (2000).
36. Ivantchev, S. et al. SUPERGROUPS—a computer program for the determination of the supergroups of the space groups. *J. Appl. Crystallogr.* **35**, 511–512 (2002).
37. Souza, I., Marzari, N. & Vanderbilt, D. Maximally localized Wannier functions for entangled energy bands. *Phys. Rev. B* **65**, 035109 (2001).



**Acknowledgements** We thank X. Dai, D. Calugaru, A. Chew, M. Vergniory and C. Chiu for discussions. We acknowledge the computational resources Cobra/Draco in the Max Planck Computing and Data Facility (MPCDF) and Atlas in the Donostia International Physics Center (DIPC). This research also used the resources of the National Energy Research Scientific Computing Center (NERSC), a US Department of Energy Office of Science User Facility operated under contract number DE-AC02-05CH11231. This work is part of a project that has received funding from the European Research Council (ERC) under the European Union's Horizon 2020 research and innovation programme (grant agreement number 101020833). B.A.B. and N.R. were also supported by the US Department of Energy (grant number DE-SC0016239), and were partially supported by the National Science Foundation (EAGER grant number DMR 1643312), a Simons Investigator grant (number 404513), the Office of Naval

Research (ONR grant number N00014-20-1-2303), the Packard Foundation, the Schmidt Fund for Innovative Research, the BSF Israel US foundation (grant number 2018226), the Gordon and Betty Moore Foundation through grant number GBMF8685 towards the Princeton theory programme, and a Guggenheim Fellowship from the John Simon Guggenheim Memorial Foundation. A.Y., N.P.O., R.J.C., L.M.S., B.A.B. and N.R. were supported by the NSF-MRSEC (grant number DMR-2011750). A.Y. was supported by NSF-DMR-1904442. B.A.B., L.M.S. and N.R. acknowledge financial support from the Schmidt DataX Fund at Princeton University made possible through a major gift from the Schmidt Futures Foundation. L.M.S. acknowledges financial support from the Packard and Sloan Foundation. B.A.B. received additional support from the Max Planck Society. L.E. was supported by the Government of the Basque Country (Project IT1301-19) and the Spanish Ministry of Science and Innovation (PID2019-106644GB-I00). C.F. was supported by the European Research Council (ERC) advanced grant number 742068 'TOP-MAT', Deutsche Forschungsgemeinschaft (DFG) through SFB 1143, and the Würzburg-Dresden Cluster of Excellence on Complexity and Topology in Quantum Matter-ct.qmat (EXC 2147, project number 390858490). S.S.P.P. acknowledges funding by the Deutsche Forschungsgemeinschaft (DFG, German Research Foundation)—project number 314790414.

**Author contributions** B.A.B. and N.R. conceived this work; N.R. and M.-R.L. performed the high-throughput calculations with the help from L.E. and Y.X.; Y.X., D.-S.M., Z.-D.S., M.-R.L., L.E. and N.R. worked out the theoretical explanations for the flat-band materials detailed in Supplementary Section F; the material lists in Supplementary Section H were manually selected by Y.X., M.-R.L., Z.-D.S., M.J. and N.R.; N.R. built the flat-band material database; D.-S.M. performed the ab initio ferromagnetic calculations advised by Y.X.; M.J., L.S. and C.F. helped curate the list of materials to find the most experimentally relevant. All authors discussed the results and wrote the main text and Methods; Y.X., Z.-D.S., M-.R.L., D.-S.M., M.J., L.E. and N.R. wrote the Supplementary Information.

**Competing interests** The authors declare no competing interests.

**Additional information**

**Supplementary information** The online version contains supplementary material available at https://doi.org/10.1038/s41586-022-04519-1.

**Correspondence and requests for materials** should be addressed to Nicolas Regnault, Yuanfeng Xu or B. Andrei Bernevig.

**Peer review information** *Nature* thanks David Carpentier and the other, anonymous, reviewer(s) for their contribution to the peer review of this work. Peer reviewer reports are available.